arXiv:1612.03842v1 [physics.atom-ph] 12 Dec 2016

# Limits on non-Newtonian gravity via state-of-the art photoassociation spectroscopy

Mateusz Borkowski,[1] Alexei A. Buchachenko,[2] Roman Ciuryło,[1] Paul S. Julienne,[3] Hirotaka Yamada,[4] Kikuchi Yuu,[4] Kekaru Takahashi,[4] Yosuke Takasu,[4] and Yoshiro Takahashi[4,5]

[1]*Institute of Physics, Faculty of Physics, Astronomy and Informatics, Nicolaus Copernicus University, Grudziadzka 5, 87-100 Torun, Poland*
[2]*Skolkovo Institute of Science and Technology, 100 Novaya Street, Skolkovo, Moscow Region, 143025, Russia*
[3]*Joint Quantum Institute, National Institute of Standards and Technology and the University of Maryland, 100 Bureau Drive, Stop 8423, Gaithersburg, Maryland 20899-8423, USA.*
[4]*Department of Physics, Graduate School of Science, Kyoto University, Kyoto 606-8502, Japan*
[5]*CREST, Japan Science and Technology Agency, Chiyoda-ku, Tokyo 102-0075, Japan*

(Dated: December 13, 2016)

A proof-of-concept determination of bounds on non-Newtonian gravity using state of the art photoassociation spectroscopy is presented. The use of Bose-Einstein condensates of ytterbium atoms rather than thermal samples and careful investigation of systematic shifts enabled the determination of a total 13 bound state energies in three isotopomers to an accuracy of ≈ 500 Hz. Several theoretical interaction potential models are proposed, including *ab initio* based, and fitted to the experimental data. Van der Waals $C_6$ coefficients for the interaction of ground state ytterbium atoms are extracted. By taking advantage of the Born-Oppenheimer approximation, which dictates that the ground state interaction potentials are the same for all isotopes we are able to give bounds on the mass-dependent non-Newtonian gravitational interaction. We show that this simple approach already gives upper bounds only three orders of magnitude larger than current best in the nanometer range and, with improved theoretical models, is a promising candidate to become a competitive method for the tightening of such bounds.

## I. INTRODUCTION

Possible non-Newtonian gravity at short distances is predicted by several theoretical models, e.g. the extra-dimensional physics with dimensional compactification in a low-energy scale or the existence of new particles [1], a run-away dilaton model [2], and a scalar Boson model [3]. Such gravity corrections are expressed by Yukawa-type terms $V_{\rm corr}(R)$ and as a result, the modified gravitational potential would have the form:

$$V_{\rm Newton}(R) + V_{\rm corr}(R) = -G\frac{m_1 m_2}{R}\left(1 + \alpha \exp(-R/\lambda)\right), \quad (1)$$

where $V_{\rm Newton}(R)$ is the usual Newtonian gravity term, $R$ is the interparticle distance, $G$ is the universal gravity constant, $m_1$ and $m_2$ are the particle masses, $\lambda$ is the interaction-range constant of Yukawa-type force, and $\alpha$ represents a coupling constant of the gravity anomaly term. There is also a close relation between the existence of anomalous gravity and the time variation of physical constants like the fine structure constant [2].

Precise tests of non-Newtonian terms in gravitational force at nanometer length scales present inherent great difficulties. To increase the accuracy of the measurement, test objects should have large mass, but it is difficult to produce samples of mesoscopic objects with high homogeneity and reproducibility. Preparing the two bodies at a controlled distance of nanometers is also problematic. Finally, the interactions in the nanometer range are dominated by the van der Waals and Casimir forces. To extract information on the much weaker gravitational forces from the measurement the precise knowledge of these forces is needed, yet for macroscopic or mesoscopic objects these interactions usually take very complicated forms which escape a complete and precise characterization.

The experimental difficulties at the nanometer scale can be overcome using microscopic particles, which has the advantage of automatically satisfying the need for both the homogeneity and reproducibility. The disadvantage is the low particle mass, which can be compensated through very precise and systematic measurements. Such approach was demonstrated recently through a systematic study of the mass dependence of scattering cross section between neutrons and various nuclei, which has revealed new limits on $\alpha$ in the range between $10^{-12}$ m and $10^{-8}$ m [4], based on the semi-empirical nuclear mass dependence of neutron scattering cross section.

Recently, an interesting approach based on the measurements of interactions in a diatomic molecule was proposed by Salumbides *et al.* [5], who considered the interactions in the $H_2$, HD, $D_2$ and $HD^+$ diatomics. The bounds on Yukawa-type forces could be obtained by a direct comparison of experimental transition energies to *ab initio* calculations. The level of experimental uncertainty is about $10^{-3}$–$10^{-4}$ cm$^{-1}$ for the neutrals and $10^{-5}$ cm$^{-1}$ for the ion, but the analysis of these light few-body systems is greatly benefited from high precision accessible in theory [6, 7]. Providing the level of accuracy comparable with experimental uncertainties, it can be used for direct calculation of the non-Newtonian gravity corrections to energy level differences. This method is useful at distances similar to the size of $H_2$ molecule, ie. on the order of $10^{-10}$ m.

We propose a complementary approach based on neutral ytterbium atoms: using two-color photoassociation (PA) spectroscopy we measure several $Yb_2$ bound state energies for different isotopes [8–11], fit mass scaled [11, 12] potential models to the experimental data and finally fit the potentials again with added Yukawa-type gravitational potentials, for different values of the interaction-range constant $\lambda$ and coupling constant $\alpha$. The values of $\alpha$, for which the quality of the fit starts deteriorating, are our limits on non-Newtonian gravity.

Within the standard Born-Oppenheimer picture, which predicts a single mass-independent $0_g^+$ internuclear potential for all isotopic varieties of $Yb_2$ dimer, this approach assigns all possible mass-dependent effects to non-Newtonian gravity assuring the strict upper bound to its magnitude. Since PA spectroscopy probes bound states close to the dissociation limit of the $Yb_2$ molecule, where the outer classical turning points are on the order of tens of atomic units, our method could provide useful limits for distances from about $10^{-10}$ m up to $10^{-7}$ m.

Yb is among the heaviest of so far laser cooled species, which increases its sensitivity to mass dependent effects. It has five bosonic isotopes, four of which have already been Bose-Einstein condensed [13–16]. The magnetic insensitivity of the ground $^1S_0$ state of Yb offers further merit for precision measurements. To achieve the high precision in our PA spectroscopy, we use Bose-Einstein condensates (BECs) [17] rather than thermal samples, which minimizes thermal broadening [18], and we also carefully characterize the systematic shifts. This way our PA spectroscopy measurements achieve unprecedently high accuracy, of the order of $2 \times 10^{-8}$ cm$^{-1}$.

The current precision of *ab initio* calculations is not enough to accurately predict the bound state energies of such a complex many-body system as $Yb_2$, therefore we resort to fitted potentials. We use both analytic and *ab initio*-based [19] potential curves to build several mass scaled potential models. By choosing the best of the potenials we can increase the accuracy of the theoretical model, which reaches $2 \times 10^{-6}$ cm$^{-1}$. Having the remaining models enable us to also study the impact of this accuracy on the bounds on non-Newtonian gravity extracted from it.

The paper is organized as follows. In Section II we describe the experimental setup used to perform photoassociation spectroscopy in Bose-Einstein condensates of ytterbium atoms. In Section III we describe the systematic shifts on photoassociation line positions that were taken into account during data analysis. The theoretical interaction models are detailed in Section IV. The determination of the bounds on non-Newtonian gravity is portrayed in Section V. We conclude the paper with Section VI.

## II. PHOTOASSOCIATION SETUP

The lowest energy levels of the Yb atom are shown in Fig. 1(a). The strong $^1S_0$-$^1P_1$ transition at 399 nm is used for Zeeman slowing. The intercombination $^1S_0$-$^3P_1$ transition at 556 nm is used for laser cooling and photoassociation spectroscopy [10, 11]. An additional laser at 532 nm is used to form a far-off optical trap (FORT). Contrary to our previous determination of the bound state energies of $Yb_2$ using two-color photoassociation spectroscopy [11], which utilized thermal atoms, we performed our measurements in BECs of $^{168}$Yb, $^{170}$Yb and $^{174}$Yb atoms. Typically $1 \times 10^4$ condensate atoms were obtained after evaporative cooling in our FORT and the atom density was around $10^{14}$ cm$^{-3}$. The procedures of creating BECs using this setup were previously published for all the investigated isotopes [13–15] and we will only describe the optical setup necessary to perform the two-color photoassociation spectroscopy.

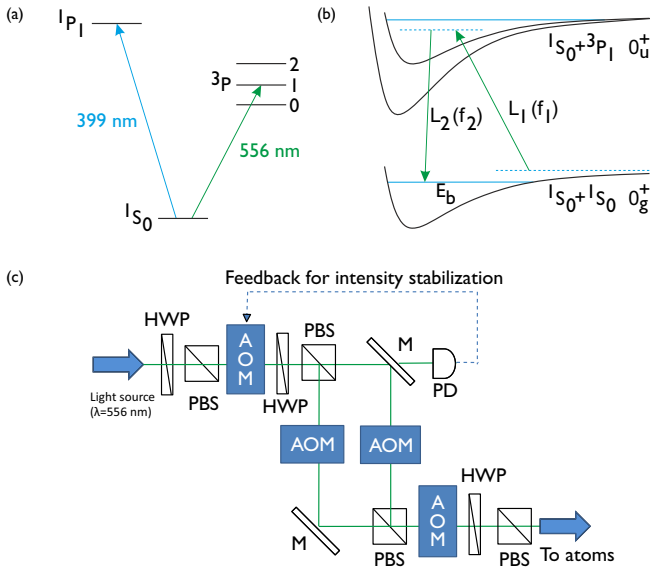


FIG. 1. (Color online) (a) Main Yb transitions used in the experiment. (b) Two-color PA spectroscopy in Raman configuration: a pair of 556 nm lasers transfer a colliding ground state atomic pair to a ground molecular bound state through a virtual excited state. The difference between the laser frequencies $f_1$-$f_2$ yields the bound state energy $E_b$. (c) Schematic setup for PA lasers. The two laser beams for the Raman transition were split by a polarized beam splitter (PBS). The frequency difference between the two beams of was controlled by acousto-optic modulators (AOMs). Two beams are combined by a PBS and then the polarization of both light were set to be parallel to each other. In order to remove PA light intensity fluctuations after optical fibers, we utilized intensity-feedback system by use of AOM and photo diode (PD). HWP: half wave plate. M: mirror.

In this experiment, pairs of colliding ground state atoms are transferred by a Raman process induced by two detuned 556 nm lasers operating near the $^1S_0 \rightarrow {}^3P_1$ transition (see Fig. 1(b)) to a bound state in the electronic molecular ground state. We observed the two-color PA signals by measuring the number of atoms remaining after the irradiation of the PA light by use of absorption imaging method with the $^1S_0$-$^1P_1$ transition. After the evaporative cooling, two lasers, $L_1$ for the free-bound transition and $L_2$ for the bound-bound transition, were simultaneously applied to the atoms in the FORT for about 30-100 ms. These beams were focused to about an 80 $\mu m$ diameter.

It follows from selection rules for a two-photon process and parity considerations we can reach vibrational states with total angular momentum of $J = 0, 2$. As we start from an $s$-wave ($J = 0$) collision, only transitions to $J = 1$ excited states are allowed – in our case bound states of the $^1S_0$+$^3P_1$ $0_u^+$ molecular state [20]. The second photon could potentially transfer the excited molecule to $J = 0, 1, 2$ ground $0_g^+$ states, but symmetry considerations for two identical bosons exclude the $J = 1$ case.

The schematic setup for the PA lasers is shown in Fig. 1(c). The two laser beams were prepared by splitting one laser beam of frequency-doubled light from a fiber laser operat-

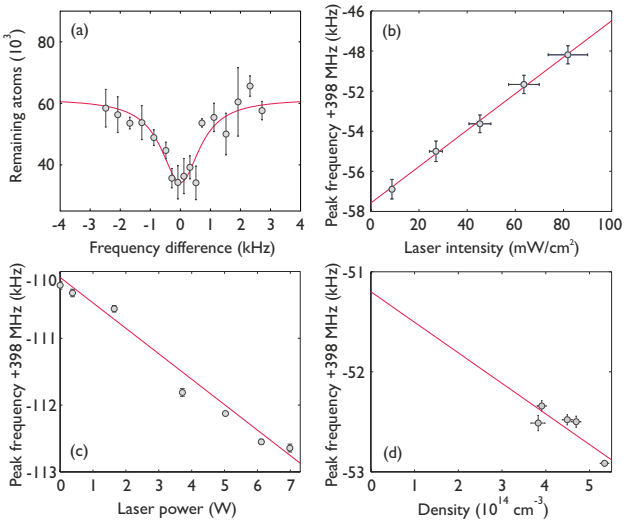


FIG. 2. (Color online) Extrapolation of the $^{170}$Yb $v = 2$, $J = 2$ line position. (a) An example two-color PA spectrum fitted with a Lorentz function; (b) light shift by PA lasers; (c) light shift by an additionally applied 532 nm laser as a function of its power; (d) mean-field shift of BEC as a function of atomic density.

ing at 1112 nm, coupled to the same optical fiber and delivered to Yb atoms. The slow drift of the laser frequency was suppressed by locking to an ultra-low expansion cavity. The laser linewidth was about 100 kHz. The frequency difference between the two beams of $L_1$ and $L_2$ was controlled by acousto-optic modulators (AOMs). The radio-frequency sources of AOMs are generated by synthesizers 8648A (Agilent, USA), which are stabilized with a 10 MHz clock from the GPS-stabilized synthesizer (DGPS-1.6, DS technology, Japan). In order to remove PA light intensity fluctuations after optical fibers, we utilized intensity-feedback system by use of an AOM and a photodiode (PD). Finally, the PA laser beams were aligned to pass through the atoms in the FORT by using a charge coupled device camera for absorption imaging. The detuning of the PA laser with respect to the atomic resonance $^1$S$_0$-$^3$P$_1$ was easily checked by observing the frequency at which the atoms in the magneto-optical trap disappeared. The frequency $f_1$ of $L_1$ was fixed at a certain detuning from a $^1$S$_0$+$^3$P$_1$ $0_u^+$ PA resonance, and the frequency $f_2$ of $L_2$ was scanned to obtain spectra of the bound states in the Yb$_2$ ground state.

## III. DETERMINATION OF BOUND STATE ENERGIES

Each PA spectrum has been fitted with a Lorentzian line shape and the observed linewidth was typically around several kHz. Peak positions suffered from systematic errors of three main origins: a light shift by two 556 nm PA lasers, a light shift by the 532 nm FORT light used to hold the atoms, and the mean-field shift of the BEC. Table I shows all of the measured binding energies in which the density shift and the light shifts from both the FORT and PA lasers are removed.

The light shift induced by the PA lasers is $\Delta E_{PA}(I_{FB}, I_{BB}) = \alpha_{FB} I_{FB} + \alpha_{BB} I_{BB}$, where $\alpha_{FB}$ and $\alpha_{BB}$ are constants related to the Franck-Condon factors for the free-bound and bound-bound transitions, respectively, and similarly $I_{FB}$ and $I_{BB}$ are the laser intensities for free-bound and bound-bound transitions. In order to compensate the light shift by extrapolation, we measured the peak positions with several laser intensities for $I_{FB}$ and $I_{BB}$ and with ratio of $I_{FB}/I_{BB}$ kept constant. Figure 2(b) shows the light shift with several intensities for $I_{BB}$ (= $I_{FB}$). We removed the light shifts by extrapolation at $I_{FB} = I_{BB} = 0$. Typical shifts by PA light were on the order of less than 10 kHz.

TABLE I. Measured binding energies $E_b$, in MHz, for homonuclear isotope pairs. Vibrational quantum numbers $v$ are numbered from the dissociation limit. $J$ is the rotational quantum number. The reported binding energies can be compared to previous measurements [11] and to the best of tested theoretical models (an *ab initio* based potential with a standard van der Waals long range interaction).

| Molecule | $v$ | $J$ | Exp. (this work) | Exp. [11] | Best model |
|---|---|---|---|---|---|
| $^{168}$Yb$_2$ | 1 | 2 | -145.53196(48) | (none) | -145.54563 |
| $^{168}$Yb$_2$ | 2 | 0 | -195.18141(46) | (none) | -195.21370 |
| $^{170}$Yb$_2$ | 1 | 2 | -3.66831(32) | -3.651(26) | -3.65756 |
| $^{170}$Yb$_2$ | 1 | 0 | -27.70024(44) | -27.661(23) | -27.65587 |
| $^{170}$Yb$_2$ | 2 | 2 | -398.05626(46) | (none) | -398.13830 |
| $^{170}$Yb$_2$ | 2 | 0 | -463.72552(80) | (none) | -463.87056 |
| $^{170}$Yb$_2$ | 3 | 2 | -1817.14074(80) | (none) | -1817.23080 |
| $^{170}$Yb$_2$ | 3 | 0 | -1922.01467(505) | (none) | -1922.32529 |
| $^{174}$Yb$_2$ | 1 | 0 | -10.62513(53) | -10.612(38) | -10.58611 |
| $^{174}$Yb$_2$ | 2 | 2 | -268.63656(56) | -268.75(21) | -268.44413 |
| $^{174}$Yb$_2$ | 2 | 0 | -325.66378(98) | -325.607(18) | -325.49548 |
| $^{174}$Yb$_2$ | 3 | 2 | -1432.82653(75) | (none) | -1432.65057 |
| $^{174}$Yb$_2$ | 3 | 0 | -1527.88543(34) | (none) | -1527.89637 |

The light shift by FORT light can be similarly eliminated, but one should be careful of the fact that changing the FORT intensity not only changes the shift by FORT light, but also changes the atom density and, consequently, the mean-field energy. Therefore, instead of directly manipulating the FORT laser intensity, we measured light shifts to the atoms in an optical lattice due to another loosely-focused light beam at the same wavelength, as shown in Fig. 2(c). The wavelength $\lambda_L$ for the optical lattice is 532 nm and the potential depth is 15 $E_R$, where $E_R = h^2/(2m\lambda_L^2)$, where $h$ is the Planck constant and $m$ is the mass of the Yb atom. With this information we estimated the light shift due to the FORT light by estimating the FORT intensity from measured trap parameters, like the trap frequencies and FORT powers. Typical shifts by 532 nm light were on the order of a few kHz.

The remaining shift is the mean-field shift of the BEC. The mean-field energy is proportional to atomic density, and therefore the shift was removed similarly by extrapolation. Typical mean-field shifts were on the order of a few kHz as shown in Fig. 2(d).

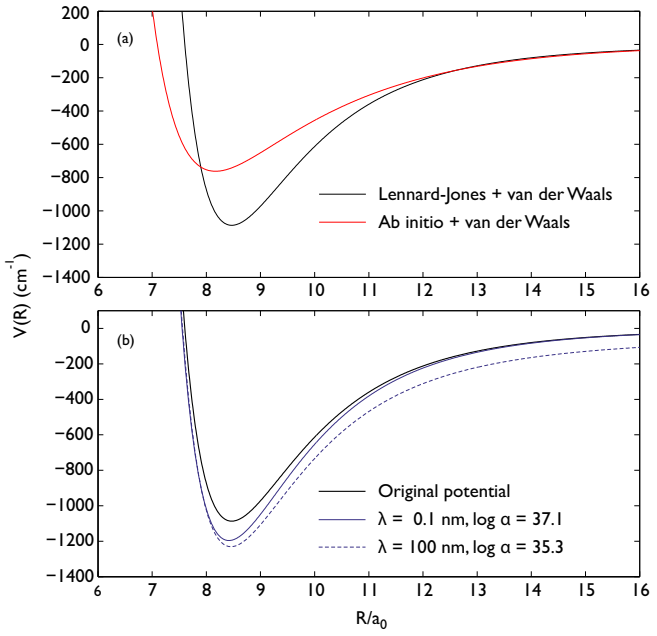


FIG. 3. (Color online) (a) Short range molecular potential models used in this study: a Lennard-Jones (black) and *ab initio* based (red) potential differing by almost a third in depth despite supporting the same number of vibrational states (72 for $^{174}$Yb). (b) The impact of the Yukawa-type gravitational terms on the atomic interaction potential. For a small value of the range parameter $\lambda = 0.1$ nm, only the short range part of the potential is affected, while for $\lambda = 100$ nm the gravitational term modifies the whole interaction.

## IV. INTERACTION MODELS

The vibrational motion in the $Yb_2$ molecule is governed by the radial Schrödinger equation of the form:

$$-\frac{\hbar^2}{2\mu}\frac{d^2}{dR^2}\Psi(R)+\mathcal{V}(R)\Psi(R)+\frac{\hbar^2 J(J+1)}{2\mu R^2}\Psi(R) = E\Psi(R) \quad (2)$$

where $J$ is the rotational quantum number, $\mu$ is the reduced mass of the molecule, and $\mathcal{V}(R)$ is Born-Oppenheimer atomic interaction potential. This equation can be solved numerically to obtain the theoretical bound state energies. The method we used is a Fourier grid Hamiltonian type discrete variable representation [21, 22] in which the $R$ variable is mapped non-linearly [23] via an exponential transformation. The resulting matrix eigenproblem is then solved using the Lanczos algorithm.

We have developed four different interaction models in order to reproduce the experimental bound state energies. The short range part of the potential could either be a simple Lennard-Jones based model potential (see Fig. 3(a)) similar to that of [11, 20]:

$$V_{LJ} = \frac{C_{12}}{R^{12}} - \frac{C_8}{R^8} - \frac{C_6}{R^6}\,, \quad (3)$$

where $C_{12}$, $C_8$ and $C_6$ are the potential parameters, or an *ab initio* [19] based potential expressed in the Tang-Toennies [24, 25] form:

$$V_{TT} = \exp(-\alpha_{TT}R - \sigma_{TT}R^2)\left(A + BR + CR^2 + D/R + ER^4\right) - \\ -\gamma_{10}(\beta_{TT}R)\frac{C_{10}}{R^{10}} - \gamma_8(\beta_{TT}R)\frac{C_8}{R^8} - \gamma_6(\beta_{TT}R)\frac{C_6}{R^6}\,, \quad (4)$$

where $\gamma_{2n}$ is a Tang-Toennies damping function of order $2n+1$. The parameters above were first fitted to the original *ab initio* potential [19] and then used as a starting point in the fitting to the experimental data.

Both potentials can be modified to include the QED Casimir-Polder effect [26] that impacts the interactions at very long range: the usual van der Waals interaction that behaves like $R^{-6}$ switches to $R^{-7}$ at very large internuclear separations. At shorter ranges it also introduces an additional $R^{-4}$ interaction. Since most of the bound states measured have their outer turning points at very long ranges, the Casimir Polder effect has measurable impact on the bound state energies. Ref. [27] gives *ab initio* corrections $f_6(R)$ and $f_8(R)$ to the $C_6R^{-6}$ and $C_8R^{-8}$ terms. In Eq. (3) we replace $C_6R^{-6}$ and $C_8R^{-8}$ with $f_6(R)C_6R^{-6}$ and $f_8(R)C_8R^{-8}$ respectively. In the case of the *ab initio* potential of Eq. (4), which used the Tang-Toennies damping functions, we have $f_6(R)\gamma_6(R)C_6R^{-6}$ and $f_8(R)\gamma_8(R)C_8R^{-8}$. The functions $f_6(R)$ and $f_8(R)$ were tabulated in [27] and here we use a cubic interpolation of the provided data. For values of $R$ outside the interpolation range the asymptotic forms $1 - f_{6,8}(R) \sim R^2$ (for small $R$) and $f_{6,8}(R) \sim R^{-1}$ (for large $R$) are used to ensure the smoothness of both functions. No QED corrections to the $C_{10}R^{-10}$ term were provided in [27]. In total we have four potential models: Lennard-Jones based (Eq. (3)) and *ab initio* based (Eq. (4));

TABLE II. Potential parameters for the two models based on the Lennard-Jones potential and the two models based on the *ab initio* potential [19].

| Lennard-Jones potentials | | |
|---|---|---|
| Parameter | van der Waals | Casimir-Polder |
| $C_{12}$ ($10^6$ a.u.) | 995.036 | 999.989 |
| $C_8$ (a.u.) | 186653 | 186638 |
| $C_6$ (a.u.) | 1921.66 | 1931.94 |
| $\chi^2$ | 607472 | 768132 |
| ***ab initio*-based potentials** | | |
| Parameter | van der Waals | Casimir-Polder |
| $\alpha_{TT}$ | 0.86685471596683 | 0.866488837743667 |
| $\beta_{TT}$ | 0.5 | 0.5 |
| $\sigma_{TT}$ | 0 | 0 |
| $C_{10}$ (a.u.) | 22411736 | 22411736 |
| $C_8$ (a.u.) | 257102 | 257073 |
| $C_6$ (a.u.) | 1940.40 | 1950.71 |
| $A$ | -261.462825518828 | -261.463586301658 |
| $B$ | 29.1954346392646 | 29.1921341886392 |
| $C$ | -1.16858320614056 | -1.16835303682871 |
| $D$ | 813.76545909246 | 813.765336806771 |
| $E$ | -0.000321690645278884 | -0.00031490206761684 |
| $\chi^2$ | 307242 | 411224 |

with either the classical van der Waals or Casimir-Polder long range interaction.

The parameters for our potential curves were obtained by a nonlinear least-squares fit of calculated bound state energies to the experiment. For the *ab initio* based curves a fit to the *ab initio* curve [19] was used as a starting point for the fitting to the experimental data. The fitted values are shown in Table II for both the model potentials and the *ab initio* based potentials. Proper mass scaling of the potentials is obtained using the procedure explained in Ref. [28]. Among the potentials with the van der Waals long range interaction, the *ab initio* based potential yields a significantly better fit ($\chi^2 = 307242$) than the simple model potential ($\chi^2 = 607472$). Similarly, with the Casimir-Polder interaction, the *ab initio* based potential ($\chi^2 = 411224$) is again better than the model potential ($\chi^2 = 768132$).

It is worth noting that the models yield differing values of the van der Waals parameter $C_6$. For the non-QED models the $C_6$ parameters are 1921.7 a.u. and 1940.4 a.u. for the Lennard-Jones and *ab initio* based potentials, respectively, and similarly the QED models yield 1931.9 a.u. and 1950.7 a.u. While the differences are on the order of 1%, given the quality of recent *ab initio* determinations [29, 30], it will be of vital importance to quantify the impact of the different forms of the interaction models on the $C_6$ coefficients extracted from PA spectroscopy. For instance, the $f_6(R)$ function at a classical turning point of 70 $a_0$, typical for the investigated bound states, reduces the effective $C_6$ coefficient by 0.44%, or by 8.5 atomic units. Coincidentally, the $C_6$ parameters extracted from van der Waals and Casimir-Polder long range models differ by about 10 atomic units. A detailed investigation, however, is beyond the scope of this work.

## V. BOUNDS ON NON-NEWTONIAN GRAVITY

To find the bounds on non-Newtonian gravity the potentials were augmented with the gravitational potential $V_{\text{Newton}} + V_{\text{corr}}$ as in Eq. (1). In this paper we assume $\alpha \geq 0$, as large negative values of $\alpha$ would result in anti-gravity at short distances. It is worth noting that the classical Newtonian part is far too weak a force to make any appreciable change in the bound state energies – it is only the Yukawa part, at its current (very large) limits, that matters. Depending on the range parameter $\lambda$, the Yukawa-type gravitational term can impact just the short range part, or the whole potential curve, as shown in Fig. 3(b). In the former case, the Yukawa potential mostly impacts the short range WKB phase of the wavefunction, which determines the position of the whole energy level series for a given isotope. In the latter case, the added potential also changes the vibrational spacings.

For each range parameter $\lambda$ a series of potential fits was carried out for steadily increasing values of the coupling constant $\alpha$. An example of the behavior of the fit quality $\chi^2$ as a function of $\alpha$ is shown in Fig. 4. In all cases $\chi^2$ would first decrease (indicating a better fit) and then quickly rise to infinity (showing a breakdown of the model). The initial decrease is to be expected – there are other small mass-dependent effects [33, 34] at work in the ytterbium dimer, and the added obviously mass-dependent Yukawa potential compensates for them. These effects are currently difficult to quantify for large systems like Yb and only just recently some preliminary estimates were published [35]. Therefore, to make sure that our limits are not underestimated, we define the threshold $\alpha_{\text{max}}$ as a point after the initial minimum where $\chi^2(\alpha_{\text{max}}) = \chi^2(\alpha = 0)$ ('X' in Fig. 4), ie. where the Yukawa-like potential *clearly* makes the fit worse. This way we choose the worst case scenario, where the non-Newtonian Yukawa potential accounts for all mass-dependent effects in a molecule. Since this is a determination of an upper bound on such forces, the resulting bounds are still correct, only more pessimistic.

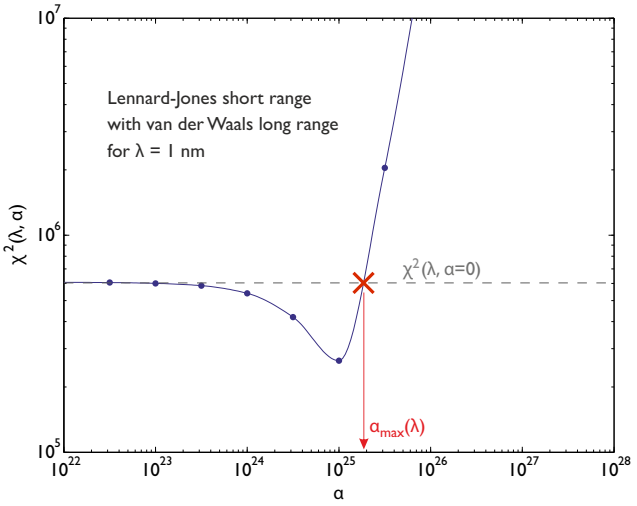


FIG. 4. (Color online) Fit quality $\chi^2(\lambda, \alpha)$ as a function of the Yukawa coupling constant $\alpha$ for a given range parameter $\lambda$ (in this example $\lambda = 1$ nm) and the simplest theoretical model of a Lennard-Jones potential with the van der Waals long range part. An 'X' marks the spot where the fit becomes worse than one without any mass dependent effects and which we take as our constraint on the Yukawa-type gravitational correction.

The limit $\alpha_{\text{max}}$ on the gravitational correction and is shown as a function of $\lambda$ in Fig. 5. The overall qualitative behavior of $\alpha_{\text{max}}$ is similar across our interaction models. For small $\lambda$ the value of $\alpha_{\text{max}}$ decreases steadily as $\lambda$ increases up until $\lambda \sim 2$ nm. For larger $\lambda$, however, $\alpha_{\text{max}}$ becomes practically independent of $\lambda$. This can be easily explained by the fact that once $\lambda$ becomes much larger than the usual internuclear distances $R$ in the Yb molecule – at most a few nm for photoassociated molecules – the gravitational correction leads to

$$\lim_{(\lambda/R)\to\infty} V_{\text{corr}} = -\alpha G \frac{m_1 m_2}{R} \tag{5}$$

which is completely independent of the range parameter $\lambda$.

The four models yield slightly different limits on the size $\alpha$ of the Yukawa-type correction to the gravitational potential. In general, models that better fit the data (ie. with lower $\chi^2$) yield better constraints on $\alpha$. For $\lambda \lesssim 1$ nm, the form of the long range atomic interaction has virtually no impact on $\alpha_{\text{max}}$. The short range form of the atomic potential (whether Lennard-Jones or *ab initio*) does matter, however, and the use of *ab*

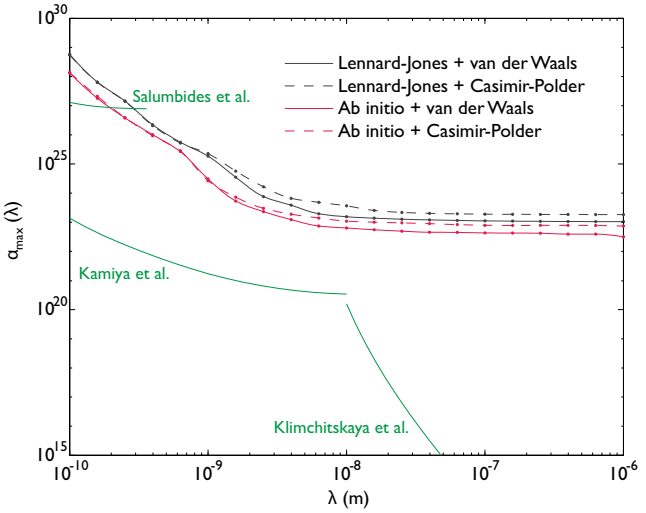


FIG. 5. (Color online) Constraints $\alpha_{\max}(\lambda)$ on the Yukawa-type corrections to the gravitational force as a function of the range parameter $\lambda$. Results for all four atomic interaction models are shown. Line style denotes the long range interaction used: solid line for a simple van der Waals ($R^{-6}$) interaction, dashed line for one that utilizes a Casimir-Polder type ($R^{-7}$ at $R \to \infty$) interaction as calculated in Ref. [27]. Line color, on the other hand, signals the short range model: black lines for Lennard-Jones and purple for *ab initio* based potentials. The asymptotic value of $\alpha_{\max}$ at large $\lambda$ is not zero in our analysis as its determination is directly related to both the theoretical and experimental errors. We also show example constraints obtained using other methods by Salumbides *et al.* [5] (from level spacings in the $HD^+$ molecule), Kamiya *et al.* [31] (scattering of neutrons on Xe), and Klimchitskaya *et al.* [32] (Casimir-Polder forces).

*initio* potentials improves the limits on $\alpha$ by half an order of magnitude. For $\lambda \gtrsim 1$ nm, however, both the short and long range forms of the potential matter.

To compare our limits on non-Newtonian gravity to those obtained using other methods, in Fig. 5 we show examples of other recent determinations. Limits from measurements of neutron scattering by Kamiya *et al.* [31] and Casimir-Polder interactions by Klimchitskaya *et al.* [32] are both more stringent than ours in their respective ranges of $\lambda$. For example at $\lambda = 10^{-8}$ m Kamiya *et al.* and Klimchitskaya *et al.* give $\log\alpha \sim 20.5$ and 20.2, respectively. In comparison, our best limit at this range is $\log\alpha \sim 22.7$, which is nearly three orders of magnitude worse. We note, however, that our current theoretical interaction models are far less accurate than the experimentally obtained values. We also note that our work is on par with (and partially improves upon) the work of Salumbides *et al.* [5] based on state-of-the-art molecular spectroscopy of the $HD^+$ molecule. Our work, however, rather than comparing *ab initio* energy levels with experiment, benefits from their mass scaling behavior [12, 28] and the multitude of available isotopes.

Better theory could yield more stringent limits. At $\lambda =$ 10 nm our Lennard-Jones+van der Waals model yields a limit on $\log\alpha \sim 23.2$, which is half an order of magnitude worse than its *ab initio* counterpart. This coincides with a factor of 2 difference in their respective values of $\chi^2$. By extrapolation, a hundredfold reduction of the $\chi^2$, or a tenfold improvement in the accuracy of the theoretical models, could already put photoassociation on par with other methods of determining the limits on non-Newtonian gravity at the nanometer scale. This will indubitably require the use of improved interaction models that take into account other mass dependent effects, like effects beyond the Born-Oppenheimer approximation [33] or the molecular isotopic effect [34]. The initial improvement of the quality of the fit as $\alpha$ is ramped up strongly corroborates this need. The vast difference between the short range potential curves used here in no way inhibits our ability to provide limits on non-Newtonian gravitational terms – it is the mass-independence of Born-Oppenheimer potentials that provides limits on gravitylike forces.

## VI. CONCLUSION

High accuracy photoassociation spectroscopy, apart from being a formidable tool for the study of atomic interactions, can also provide useful limits on non-Newtonian gravity. Our proof-of-concept determination yielded bounds on Yukawa-type corrections for the nanometer range that are only three orders of magnitude larger than the current best obtained from neutron scattering. Thanks to our multiple theoretical models we could also show that, as atomic interaction models improve, these bounds tighten very rapidly – a tenfold improvement in accuracy could already put our method on par with other methods used in the nanometer range. This could be achieved in the future by including the currently difficult to calculate mass-dependent molecular effects.

## ACKNOWLEDGMENTS

We acknowledge K. Enomoto, M. Ando, J. Hutson, and E. Tiemann for their useful comments. This work has been partially supported by the Grant-in-Aid for Scientific Research of JSPS (25220711, 26247064) and Impulsing Paradigm Changing Through Disruptive Technologies (ImPACT) program. This research was partially supported by the TEAM Programme of the Foundation for Polish Science, co-financed by the EU European Regional Development Fund and by the COST Action CM1405 MOLIM, and also by the National Science Centre grant no. UMO-2014/13/N/ST2/02591. It is part of an ongoing research program of the National Laboratory FAMO in Toruń, Poland. Calculations have been carried out in Wroclaw Centre for Networking and Supercomputing grant no. 353.

[1] E. Adelberger, B. Heckel, and A. Nelson, Annual Review of Nuclear and Particle Science **53**, 77 (2003).

[2] T. Damour, Astrophysics and Space Science **283**, 445 (2003).

[3] Y. Su, B. R. Heckel, E. G. Adelberger, J. H. Gundlach, M. Harris, G. L. Smith, and H. E. Swanson, Phys. Rev. D **50**, 3614 (1994).

[4] V. V. Nesvizhevsky, G. Pignol, and K. V. Protasov, Phys. Rev. D **77**, 034020 (2008).

[5] E. J. Salumbides, J. C. J. Koelemeij, J. Komasa, K. Pachucki, K. S. E. Eikema, and W. Ubachs, Phys. Rev. D **87**, 112008 (2013).

[6] K. Pachucki and J. Komasa, The Journal of Chemical Physics **130**, 164113 (2009), http://dx.doi.org/10.1063/1.3114680.

[7] K. Pachucki, Phys. Rev. A **82**, 032509 (2010).

[8] K. M. Jones, E. Tiesinga, P. D. Lett, and P. S. Julienne, Reviews of Modern Physics **78**, 483 (2006).

[9] J. L. Bohn and P. S. Julienne, Phys. Rev. A **60**, 414 (1999).

[10] S. Tojo, M. Kitagawa, K. Enomoto, Y. Kato, Y. Takasu, M. Kumakura, and Y. Takahashi, Physical Review Letters **96**, 153201 (2006).

[11] M. Kitagawa, K. Enomoto, K. Kasa, Y. Takahashi, R. Ciuryło, P. Naidon, and P. S. Julienne, Phys. Rev. A **77**, 012719 (2008).

[12] G. F. Gribakin and V. V. Flambaum, Phys. Rev. A **48**, 546 (1993).

[13] Y. Takasu, K. Maki, K. Komori, T. Takano, K. Honda, M. Kumakura, T. Yabuzaki, and Y. Takahashi, Physical Review Letters **91**, 040404 (2003).

[14] T. Fukuhara, S. Sugawa, and Y. Takahashi, Phys. Rev. A **76**, 051604 (2007), arXiv:0709.3068.

[15] S. Sugawa, R. Yamazaki, S. Taie, and Y. Takahashi, Phys. Rev. A **84**, 011610 (2011).

[16] T. Fukuhara, S. Sugawa, Y. Takasu, and Y. Takahashi, Phys. Rev. A **79**, 021601 (2009), arXiv:0811.0671.

[17] Y. Takasu, K. Honda, K. Komori, T. Kuwamoto, M. Kumakura, Y. Takahashi, and T. Yabuzaki, Physical Review Letters **90**, 023003 (2003).

[18] K. M. Jones, P. D. Lett, E. Tiesinga, and P. S. Julienne, Phys. Rev. A **61**, 012501 (2000).

[19] A. A. Buchachenko, G. Chałasiński, and M. M. Szczęśniak, European Physical Journal D **45**, 147 (2007).

[20] M. Borkowski, R. Ciuryło, P. S. Julienne, S. Tojo, K. Enomoto, and Y. Takahashi, Phys. Rev. A **80**, 012715 (2009).

[21] R. Meyer, The Journal of Chemical Physics **52**, 2053 (1970).

[22] D. T. Colbert and W. H. Miller, The Journal of Chemical Physics **96**, 1982 (1992).

[23] E. Tiesinga, C. J. Williams, and P. S. Julienne, Phys. Rev. A **57**, 4257 (1998).

[24] K. T. Tang and J. P. Toennies, J. Chem. Phys. **80**, 3726 (1984).

[25] K. Patkowski, V. Špirko, and K. Szalewicz, Science **326**, 1382 (2009).

[26] H. B. Casimir and D. Polder, Physical Review **73**, 360 (1948).

[27] P. Zhang and A. Dalgarno, Molecular Physics: An International Journal at the Interface Between Chemistry and Physics **106**, 1525 (2008).

[28] M. Borkowski, P. S. Żuchowski, R. Ciuryło, P. S. Julienne, D. Kędziera, L. Mentel, P. Tecmer, F. Münchow, C. Bruni, and A. Görlitz, Phys. Rev. A **88**, 052708 (2013).

[29] M. S. Safronova, S. G. Porsev, and C. W. Clark, Physical Review Letters **109**, 230802 (2012).

[30] S. G. Porsev, M. S. Safronova, A. Derevianko, and C. W. Clark, Physical Review A **89**, 012711 (2014).

[31] Y. Kamiya, K. Itagaki, M. Tani, G. N. Kim, and S. Komamiya, Physical Review Letters **114**, 161101 (2015).

[32] G. L. Klimchitskaya, U. Mohideen, and V. M. Mostepanenko, Phys. Rev. D **87**, 125031 (2013).

[33] M. Przybytek and B. Jeziorski, Chemical Physics **401**, 170 (2012), recent advances in electron correlation methods and applications.

[34] J. Schlembach and E. Tiemann, Chemical Physics **68**, 21 (1982).

[35] J. J. Lutz and J. M. Hutson, Journal of Molecular Spectroscopy (2016), http://dx.doi.org/10.1016/j.jms.2016.08.007, (in press).